Calibration of parameters for a discrete element model of cotton field residual film-soil mixtures

Jinming Li[1,2], Jiaxi Zhang[1,2*], Yichao Wang[1,2], Zebin Gao[1,2], Xiaoxuan Wang[1,2], Shilong Shen[1,2]

(1. *College of Mechanical and Electrical Engineering, Xinjiang Agricultural University, Urumqi 830052, China*;
2. *Key Laboratory of Xinjiang Intelligent Agricultural Equipment, Xinjiang Agricultural University, Urumqi 830052, China*)

Abstract: During residual film recovery operations, the mixing of residual film with soil and the absence of accurate interaction parameters significantly hinder the optimization of key machinery components. To tackle this issue, this study develops a discrete element simulation model based on the Hertz–Mindlin with JKR (Johnson-Kendall-Roberts) contact model, using the residual film-soil mixture as the simulated material. The contact parameters were calibrated through a combination of physical experiments and EDEM simulations. Using Design-Expert software, angle of repose tests and Plackett–Burman experiments were carried out to identify the parameters that have a significant influence on the angle of repose. The optimal set of parameters was determined through steepest ascent and Box–Behnken design (BBD) experiments: residual film–soil rolling friction coefficient 0.61, soil–soil rolling friction coefficient 0.60, soil–steel static friction coefficient 0.68, and soil JKR surface energy 0.46 J/m^2. Validation results indicate relative errors of 4.58% for the angle of repose and 2.58% for the uniaxial compressive strength between simulated and measured values. These outcomes offer a useful reference for optimizing residual film recovery equipment and for modeling soil–residual film composite materials.

Keywords: cotton fields, residual film-soil mixture, parameter calibration, angle of repose, discrete element method, uniaxial compression test

DOI: 10.25165/j.ijabe.20261901.10197

Citation: Li J M, Zhang J X, Wang Y C, Gao Z B, Wang X X, Shen S L. Calibration of parameters for a discrete element model of cotton field residual film-soil mixtures. Int J Agric & Biol Eng, 2026; 19(1): 59–66.

1 Introduction

The widespread use of plastic film mulching technology in cotton fields in Xinjiang has significantly increased cotton yield and quality, but has also led to serious pollution from residual plastic film[1]. Mechanized recovery is an effective approach to improve soil structure and reduce environmental pollution. However, during the recovery process, the mixing of residual plastic film with soil and the lack of accurate interaction parameters greatly hinder the optimization of key components in film recovery machinery, leading to a high impurity rate in the recovered materials. Therefore, systematic research on the physical properties of residual film-soil mixtures is urgently needed. Since conventional experimental methods have difficulty accurately obtaining relevant contact parameters[2], the introduction of discrete element simulation technology to model the interaction between soil and residual film can provide important theoretical foundations and technical support for optimizing the structure of residual film recovery machinery and for modeling residual film-soil mixture.

In recent years, the discrete element method (DEM) has been extensively applied to model and calibrate the parameters of various agricultural particulate systems[3]. Researchers have successfully developed DEM models for a range of single plant components, such as Ligier et al.[4], who employed the multi-sphere method to construct a DEM model of maize kernels and calibrated its key parameters. Han et al.[5] utilized DEM to validate contact parameters for soybeans. Shi et al.[6] constructed a flexible model of flax stems using a DEM bonding model and calibrated its parameters to simulate the shearing process of flax stems. Du et al.[7] conducted tensile and puncture tests on a DEM mechanical model of tea stems. Han et al.[8] established a discrete element model for moist sand particles and calibrated its key parameters. Ma et al.[9] employed a delayed elasticity model and linear adhesion model to develop a soil particle discrete element model, calibrating soil parameters. Tian et al.[2] created a moving discrete element model for maize stover-soil mixtures, calibrating contact parameters via angle of repose. Ma et al.[10] employed the discrete element method to establish a simulation model for maize stover and cattle manure mixtures, validating parameters through uniaxial compression tests. Yao et al.[11] developed a soil-root-stover discrete element model, verifying contact parameters using the angle of repose. Despite these advances in modeling various agricultural composites, a significant research gap persists. There is a notable scarcity of research dedicated to the simulation and parameter calibration of soil-residual film mixtures, which is the focus of this work.

This research focuses on the parameter calibration of residual film-soil mixtures found in Xinjiang's cotton fields. By combining physical experiments with numerical simulations, the contact parameters for the residual film-soil mixture were calibrated using EDEM software. The angle of repose, selected as the key response variable, was measured using image processing techniques. Subsequently, a series of Plackett-Burman screening, steepest ascent (ramp), and Box-Behnken response surface tests were conducted to determine the optimal discrete element parameters for

Received date: 2025-09-17 **Accepted date:** 2025-12-09

Biographies: Jinming Li, PhD candidate, research interest: recycling agriculture technology and equipment, Email: xjaujinmingli@163.com; **Yichao Wang**, PhD, research interest: harvesting machinery, Email: 360318122@qq.com; **Zebin Gao**, MS, research interest: recycling agriculture technology and equipment, Email: 287024453@qq.com; **Xiaoxuan Wang**, MS, research interest: recycling agriculture technology and equipment, Email: wxxazjm@163.com; **Shilong Shen**, PhD, research interest: recycling agriculture technology and equipment, Email: 2505770715@qq.com.

***Corresponding author: Jiaxi Zhang**, Professor, research interest: recycling agriculture technology and equipment research. College of Mechanical and Electrical Engineering, Xinjiang Agricultural University, Urumqi 830052, Email: zhangjiaxi@xjau.edu.cn.

the mixture[12]. Finally, the reliability of these calibrated parameters was validated against physical angle of repose and uniaxial compression tests. This process establishes a validated foundation for constructing an accurate discrete element model of the residual film-soil mixture.

2 Materials and methods

2.1 Test materials

The experimental materials were sourced from a cotton farm in Yuli County, Bayingolin Mongol Autonomous Prefecture, Xinjiang Uygur Autonomous Region, characterized by a sandy loam soil type. Following the autumn film recovery, composite samples of the residual film-soil mixture were collected using a standard five-point sampling method. The samples were then processed in the laboratory. The density of both soil and film was measured separately. Soil moisture content was determined via the drying method. The dried soil was sieved, with the dominant fraction (93.25%) falling within the 0-2 mm particle size range. Concurrently, the separated film was washed and cut into small, uniform strips. The final configuration of the simulated film-soil sample is depicted in Figure 1.

2.2 Test method

To calibrate the discrete element parameters for a residual film-soil mixture, a methodology integrating physical and simulated tests was employed. Initially, the mean angle of repose of the mixture was determined through physical experiments on a dedicated testing rig. In parallel, simulations were conducted in EDEM 2022. A Plackett-Burman test, designed in Design-Expert 13.0, was performed to screen for parameters with a significant influence on the simulated angle of repose[13,14]. Next, the steepest ascent method was used to efficiently locate the optimal region for these factors. Subsequently, a Box-Behnken Design (BBD) was implemented to construct a response surface regression model. This model was then optimized to derive the ideal combination of parameters[15-17]. Finally, a validation test was run using this optimal parameter set, and the simulated angle of repose was compared against the experimental result to verify the accuracy of the calibrated model.

2.3 Residual film-soil mixture angle of repose physical test

The physical angle of repose for the residual film-soil mixture was measured using a custom testing rig, as depicted in Figure 2. The apparatus consists of a hopper, a support frame, and a steel base plate. During each trial, the mixture was released from the hopper onto the plate. Once the resulting pile stabilized, a frontal photograph was captured with a smartphone mounted perpendicular to the frame. To ensure measurement accuracy, the captured images were processed in MATLAB. This involved binarization and contour extraction to precisely define the pile's edges[18-21]. The resulting edge data was imported into Origin, where linear fitting was applied to both slopes of the pile to calculate the angle of repose (Figure 5). The experiment was replicated 10 times, and the average value was calculated. The mean physical angle of repose for the mixture was determined to be 29.80°.

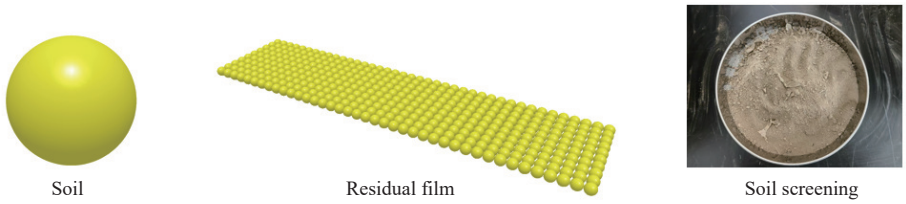

Figure 1 Simulation model of residual film and soil sample

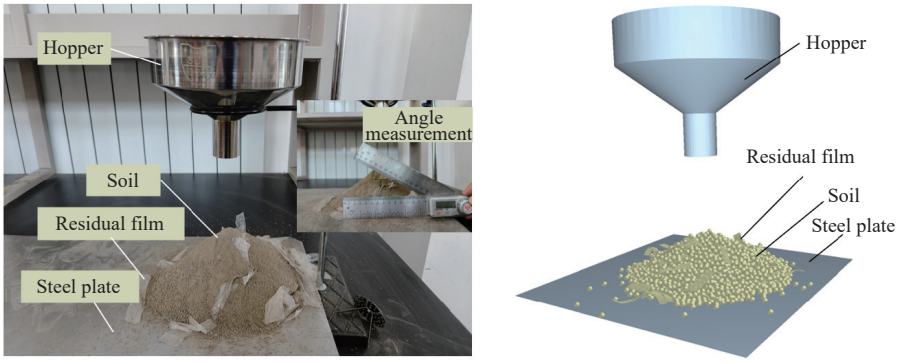

a. Physical test angle of repose measurement b. Simulated angle of repose test

Figure 2 Angle of repose measurement

3 Angle of repose simulation test

3.1 Selection of contact model

A key characteristic of residual film-soil mixtures is their inherent particle adhesion, which is primarily attributed to the electrostatic nature of the residual film. The Hertz-Mindlin with JKR contact model is specifically designed to simulate such cohesive behaviors by incorporating interparticle attractive forces[22]. Consequently, this model was employed to construct the discrete element representation of the film-soil mixture in this study.

The JKR model quantifies the normal elastic contact force F_{JKR} that arises from particle interaction and surface deformation, a process depicted in Figure 3. This force is primarily determined by two key parameters: the normal overlap (δ) and the surface energy (γ)[18]. The relationship is expressed by the following equation:

$$\begin{cases} F_{JKR} = -4\sqrt{\pi\gamma E^*}\alpha^{\frac{3}{2}} + \dfrac{4E^*}{3R^*}\alpha^3 \\ \delta = \dfrac{\alpha^2}{R^*} - \sqrt{\dfrac{4\pi\gamma\alpha}{E^*}} \end{cases} \tag{1}$$

Among them

$$\frac{1}{E^*} = \frac{1-\nu_1^2}{E_1} + \frac{1-\nu_2^2}{E_2} \tag{2}$$

$$R^* = \frac{1}{R_1} - \frac{1}{R_2} \tag{3}$$

where, F_{JKR} is the normal elastic force in the model, N; δ is the normal overlap between two contacting particles, m; α is the tangential overlap between two contacting particles, m; γ is the surface energy, N/m; E^* is the equivalent Young's modulus, Pa; R^* is the equivalent contact radius, m; v_1 and v_2 are the Poisson's ratios of the two particles; E_1 and E_2 are the shear moduli of the two contacting particles, Pa; R_1 and R_2 are the radii of the two contacting particles, m.

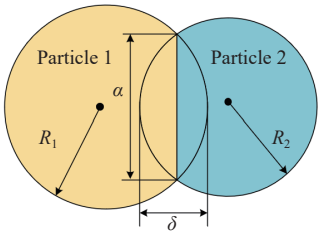

Figure 3 Schematic diagram of Hertz-Mindlin with JKR contact model principle

When the surface energy γ=0, the normal force F_n in the F_{JKR} model is equal to that in the Hertz-Mindlin contact model, i.e.,

$$F_{JKR} = F_n = \frac{4}{3}E^* \sqrt{R^*}\delta^{\frac{3}{2}} \tag{4}$$

If particles are not in direct contact, the JKR model can also provide attractive cohesive forces[13], with the maximum gap for non-zero cohesive forces between particles being:

$$\delta_c = \frac{\alpha_c^2}{R^*} - \sqrt{\frac{4\pi\gamma\alpha_c}{E^*}} \tag{5}$$

$$\alpha_c = \left[\frac{9\pi\gamma R^*}{2E^*} - \left(\frac{3}{4} - \frac{1}{\sqrt{2}}\right)\right]^{\frac{1}{3}} \tag{6}$$

where, δ_c represents the maximum normal gap between particles when nonzero cohesive forces exist, m; α_c denotes the maximum tangential gap between particles when nonzero cohesive forces exist, m.

When $\delta > \delta_c$, the cohesive force between particles becomes zero.

When particles are not in actual contact and separated by a distance equal to δ_c, cohesive force reaches its maximum value.

$$F_{\text{pull-off}} = -\frac{3}{2}\pi\gamma R^* \tag{7}$$

where, $F_{\text{pull-off}}$ represents the cohesive force between two particles, N.

3.2 Simulation model development

The angle of repose simulation was set up in EDEM 2022. A three-dimensional hopper model, created in SolidWorks, was imported as an STL file. The steel base plate was generated internally using EDEM's Polygon feature, with its material properties defined as per Table 1. Two particle factories were established above the hopper to dynamically generate soil and residual film particles under gravity (9.81 m/s^2)[23,24]. The residual film was modeled as flexible strips by bonding 0.5 mm radius spheres together, providing a computationally efficient representation. After the mixture settled into a stable pile on the steel plate (Figure 4), the angle of repose was measured in the post-

Table 1 Material intrinsic parameters

Parameters	Values
Soil Poisson's ratio	0.36
Soil shear modulus/Pa	1×10^6
Residual Poisson's ratio	0.32
Residual film shear modulus/Pa	1.57×10^6
Steel Poisson's ratio	0.3
Steel shear modulus/Pa	7.8×10^{10}
Steel density/kg·m^{-3}	7850

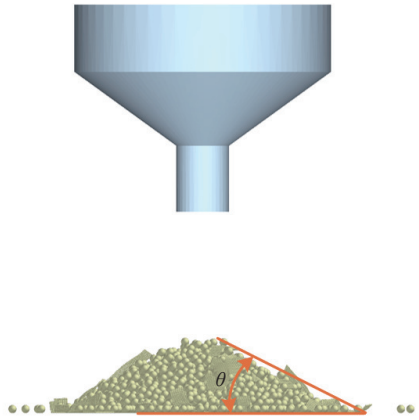

Figure 4 Simulation test of repose angle

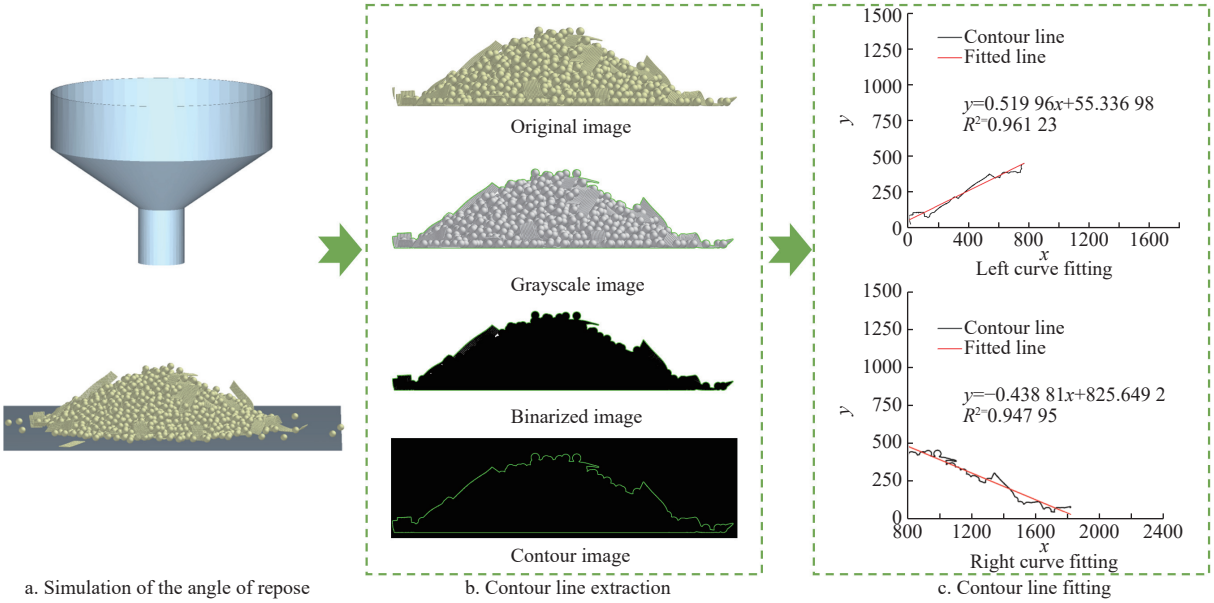

a. Simulation of the angle of repose b. Contour line extraction c. Contour line fitting

Figure 5 Extraction and fitting of simulated angle of repose profiles

processor by applying a three-point protractor tool to the pile's cross-section[25,26]. The initial range of contact parameters used in the simulation is listed in Table 2.

Table 2 Parameters and level required in DEM simulation

Parameters	Levels		
	–1	0	1
Residual film-soil recovery coefficient X_1	0.25	0.45	0.65
Residual film-soil static friction coefficient X_2	0.40	0.50	0.60
Residual film-soil rolling friction coefficient X_3	0.35	0.55	0.75
Soil-soil recovery coefficient X_4	0.15	0.45	0.75
Soil-soil static friction coefficient X_5	0.16	0.50	0.84
Soil-soil rolling friction coefficient X_6	0.10	0.40	0.70
Soil-steel static friction coefficient X_7	0.40	0.60	0.80
Soil-steel rolling friction coefficient X_8	0.15	0.20	0.25
Soil JKR surface energy X_9/(J·m^{-2})	0.20	0.40	0.60
Residual film-soil JKR surface energy X_{10}/(J·m^{-2})	0.30	0.40	0.50

4 Test and result analysis

4.1 Plackett-Burman test

To identify the most influential simulation parameters, a Plackett-Burman screening design was implemented using Design-Expert 13.0 software. The angle of repose of the residual film-soil mixture was designated as the primary response variable[27]. The experimental design consisted of 12 groups, evaluating the ten factors listed in Table 3 (X_1–X_{10}), which include various coefficients of restitution, friction, and JKR surface energy; k denotes the dummy blank column. An analysis of variance (ANOVA) was performed to determine the significance of each factor. The results, presented in Table 4, rank the factors by their effect on the angle of repose. The order of significance was determined to be X_7>X_6>X_3>X_9>X_2>X_4>X_8>X_{10}>X_1>X_5. Notably, the top four factors—the soil-steel static friction coefficient (X_7), soil-soil rolling friction coefficient (X_6), residual film-soil rolling friction coefficient (X_3), and soil JKR surface energy (X_9)—collectively contributed to 90.46% of the observed variation. All other factors had individual contributions of less than 5%. Consequently, these four highly significant parameters were chosen for further optimization using the method of steepest ascent[28].

The statistical analysis in Table 4 confirms the significance and robustness of the model. The overall model is highly significant (p<0.05) and demonstrates an exceptional goodness of fit, with a coefficient of determination (R^2) of 0.9998 and an adjusted R^2 of 0.9973. The R^2 value, approaching 1, demonstrates strong model correlation[29]. Furthermore, the experiment's high precision and reliability are confirmed by a low coefficient of variation (CV= 0.6829%). Among the tested parameters, the p-values for X_3, X_6, X_7, and X_9 were all less than 0.05, identifying them as the factors with a statistically significant influence on the angle of repose.

Table 3 Results of Plackett-Burman design test

Test number	Factor											Angle of repose/θ(°)
	X_1	X_2	X_3	X_4	X_5	X_6	X_7	X_8	X_9	X_{10}	k	
1	–1	1	1	1	–1	–1	–1	1	–1	1	1	23.25
2	–1	–1	–1	1	–1	1	1	–1	1	1	1	29.67
3	1	1	–1	–1	–1	1	–1	1	1	–1	1	26.34
4	–1	1	–1	1	1	–1	1	1	1	–1	–1	25.12
5	1	1	–1	1	1	1	–1	–1	–1	1	–1	25.29
6	1	–1	1	1	–1	1	1	1	–1	–1	–1	28.93
7	1	1	1	–1	–1	–1	1	–1	1	1	–1	31.05
8	–1	1	1	–1	1	1	1	–1	–1	–1	1	32.19
9	1	–1	–1	–1	1	–1	1	1	–1	1	1	24.38
10	–1	–1	1	–1	1	1	–1	1	1	1	–1	28.76
11	1	–1	1	1	1	–1	–1	–1	1	–1	1	24.27
12	–1	–1	–1	–1	–1	–1	–1	–1	–1	–1	–1	20.32

Table 4 Analysis of Plackett-Burman design test results

Experimental factors	Effect	Mean square	Contribution level/%	p	Significance ranking
X_1	0.16	0.0752	0.05	0.3728	9
X_2	1.15	3.9800	2.94	0.0579	5
X_3	2.89	25.0300	18.46	0.0231	3
X_4	–1.09	3.5300	2.61	0.0614	6
X_5	0.08	0.0169	0.01	0.6051	10
X_6	3.80	43.2800	31.93	0.0176	2
X_7	3.85	44.5100	32.83	0.0174	1
X_8	–1.00	3.0100	2.22	0.0665	7
X_9	1.81	9.8100	7.24	0.0369	4
X_{10}	0.87	2.2800	1.68	0.0763	8

A visual analysis of the Plackett-Burman results was conducted using a semi-normal probability plot and a Pareto chart, as presented in Figure 6. In the semi-normal plot (Figure 6a), the significance of a factor is indicated by its distance from the fitted line of null effects. Factors X_3, X_6, X_7, and X_9 are positioned far from this line, clearly identifying them as the most influential parameters.

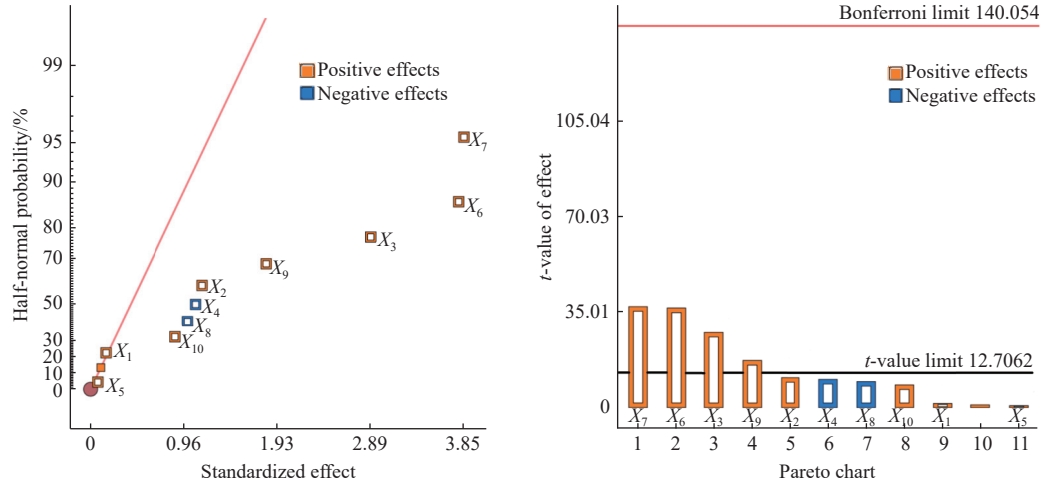

a. Half-normal probability effect diagram of standardized effect b. Pareto chart

Figure 6 Analysis of significant effects from the Plackett-Burman experiment results

All four demonstrate a positive effect on the angle of repose, with the magnitudes of X_6 and X_7 being substantially greater than those of X_3 and X_9. The Pareto chart (Figure 6b) provides further confirmation. The standardized effects for factors X_3, X_6, X_7, and X_9 all surpass the Bonferroni limit, again highlighting their statistical significance. Based on these conclusive results, all non-significant factors were held constant at their central values for the remainder of the study (X_1=0.45, X_2=0.5, X_4=0.45, X_5=0.5, X_8=0.2, and X_{10}=0.4).

4.2 Steepest ascent experiment

Based on the results of the Plackett-Burman test, a steepest ascent experiment was designed to efficiently locate the optimal response region for the four most significant factors: the soil-steel static friction coefficient (X_7), soil-soil rolling friction coefficient (X_6), residual film-soil rolling friction coefficient (X_3), and soil JKR surface energy (X_9). Non-significant parameters were fixed at their intermediate levels. The experimental design and corresponding results are summarized in Table 5. The performance of each parameter set was evaluated by the relative error (Y_1) between the simulated angle of repose (θ') and the measured physical angle (θ), as defined in Equation (8). The analysis revealed that the fourth set of parameters minimized this relative error. Therefore, this set was chosen as the central level (0) for the next stage of optimization. The values from the preceding (third) and succeeding (fifth) experimental groups were designated as the low (–1) and high (+1) levels, respectively, for the upcoming Box-Behnken Design (BBD)[30]. The factor level coding is provided in Table 6.

$$Y = \frac{|\theta_S - \theta|}{\theta} \times 100\% \tag{8}$$

where, Y is the relative error of the angle of repose, %; θ_S is the simulated angle of repose, (°); θ is the actual angle of repose, (°).

Table 5 Design and results of climbing test

Test number	X_3	X_6	X_7	X_9/(J·m^{-2})	Angle of repose/θ(°)	Relative error Y/%
1	0.35	0.10	0.40	0.20	24.39	16.98
2	0.45	0.25	0.50	0.30	26.46	11.21
3	0.55	0.40	0.60	0.40	31.86	6.91
4	0.65	0.55	0.70	0.50	28.63	3.93
5	0.75	0.70	0.80	0.60	32.86	10.27

Table 6 BBD test factors and levels coding

Encoding	Factor			
	X_3	X_6	X_7	X_9/(J·m^{-2})
–1	0.55	0.40	0.6	0.40
0	0.65	0.55	0.7	0.50
1	0.75	0.70	0.8	0.60

4.3 Box-Behnken test

To optimize the four significant parameters (X_3, X_6, X_7, and X_9), a Box-Behnken Design (BBD) was implemented. This four-factor, three-level experiment used the angle of repose as the response metric and comprised a total of 29 trials, with factor levels informed by the steepest ascent results. The experimental design and results are detailed in Table 7, while the corresponding analysis of variance (ANOVA) is presented in Table 8[31].

4.4 Interaction effect analysis in regression models

Using Design-Expert 13.0, a second-order polynomial regression model was established through an analysis of variance (ANOVA) of the experimental results. This model defines the relationship between the angle of repose and the four experimental factors, as expressed in the following equation:

Table 7 Test scheme and results

Test number	Factor				Angle of repose/θ(°)
	X_3	X_6	X_7	X_9/(J·m^{-2})	
1	0	1	0	1	29.44
2	–1	1	0	0	31.41
3	1	0	1	0	29.93
4	0	–1	1	0	31.46
5	1	–1	0	0	28.95
6	0	1	–1	0	29.79
7	0	1	0	–1	31.88
8	0	0	1	–1	32.27
9	0	0	0	0	29.14
10	0	1	1	0	30.24
11	–1	–1	0	0	28.53
12	0	0	0	0	29.97
13	1	0	0	1	28.12
14	1	0	0	–1	31.47
15	0	–1	0	1	30.63
16	–1	0	1	0	30.98
17	0	0	1	1	28.25
18	1	0	–1	0	26.44
19	0	–1	–1	0	25.32
20	0	0	0	0	29.93
21	1	1	0	0	29.47
22	0	0	–1	1	27.32
23	–1	0	–1	0	25.41
24	0	0	0	0	29.93
25	0	0	0	0	29.76
26	–1	0	0	–1	28.34
27	0	0	–1	–1	26.54
28	–1	0	0	1	29.26
29	0	–1	0	–1	27.89

Table 8 ANOVA of quadratic model

Sources of variance	Sum of squares	Degree of freedom	Mean square	F-value	p-value	Significance
Model	88.72	14	6.34	17.95	<0.0001	**
X_3	0.0169	1	0.0169	0.0478	0.8301	-
X_6	7.44	1	7.44	21.08	0.0004	**
X_7	41.48	1	41.48	117.49	<0.0001	**
X_9	2.40	1	2.40	6.81	0.0206	*
X_3X_6	1.39	1	1.39	3.94	0.0670	-
X_3X_7	1.08	1	1.08	3.06	0.1019	-
X_3X_9	4.56	1	4.56	12.91	0.0029	**
X_6X_7	8.09	1	8.09	22.93	0.0003	**
X_6X_9	6.71	1	6.71	19.00	0.0007	**
X_7X_9	5.76	1	5.76	16.32	0.0012	**
X_3^2	1.45	1	1.45	4.12	0.0619	-
X_6^2	0.8598	1	0.8598	2.44	0.1409	-
X_7^2	6.73	1	6.73	19.06	0.0006	**
X_9^2	0.0479	1	0.0479	0.1356	0.7182	-
Residual	4.94	14	0.3530	-	-	-
Lack of fit	4.46	10	0.4457	3.67	0.1107	-
Pure error	0.4853	4	0.1213	-	-	-
Cor total	93.66	28	-	-	-	-

Note: * indicates a significant impact (0.01<p<0.05); ** indicates that the effect is extremely significant (p≤0.01).

$$\theta = 29.75 + 0.7875X_6 + 1.86X_7 - 0.4475X_9 - 1.07X_3X_9 - 1.42X_6X_7 - 1.29X_6X_9 - 1.2X_7X_9 - 1.02X_7^2 \quad (9)$$

The variance analysis of the experimental regression model is listed in Table 8. The regression model is highly significant ($p<0.0001$) with the coefficient of determination R^2 is 0.9472, which indicating a good fit of the regression equation; And the coefficient of variation is 2.03%, demonstrating high reliability of this experiment. This indicates the model effectively reflects the relationship between the angle of repose and residual film-soil rolling friction coefficient X_3, soil-soil rolling friction coefficient X_6, soil-steel static friction coefficient X_7, and soil JKR surface energy X_9. The model F-value reveals the influence order of the four experimental factors on the angle of repose, from greatest to least: X_7, X_6, X_3, X_9. Among these, X_6, X_7, X_3X_9, X_6X_7, X_6X_9, X_7X_9, and X_7^2 exerted extremely significant effects on the angle of repose; X_9 had a significant effect; while X_3, X_3X_6, X_3X_7, X_3^2, X_6^2, and X_9^2 showed no significant influence.

Response surface plots illustrating the interaction effects on the angle of repose were generated using Design-Expert 13.0 and are presented in Figure 7. The steepness of a curve on these plots corresponds to the magnitude of the factor's influence. By visually inspecting the plots, the relative impact of the interacting factors can be determined. Figure 7b and Figure 7d clearly show that the response surface for the soil-steel static friction coefficient (X_7) is steeper than that for both the soil-soil rolling friction coefficient (X_6) and the soil JKR surface energy (X_9), indicating its dominant effect. Similarly, the curves for X_6 (Figure 7c) and X_9 (Figure 7a) are also significant, with X_6 having a greater influence than X_9. These visual results corroborate the statistical findings from the ANOVA.

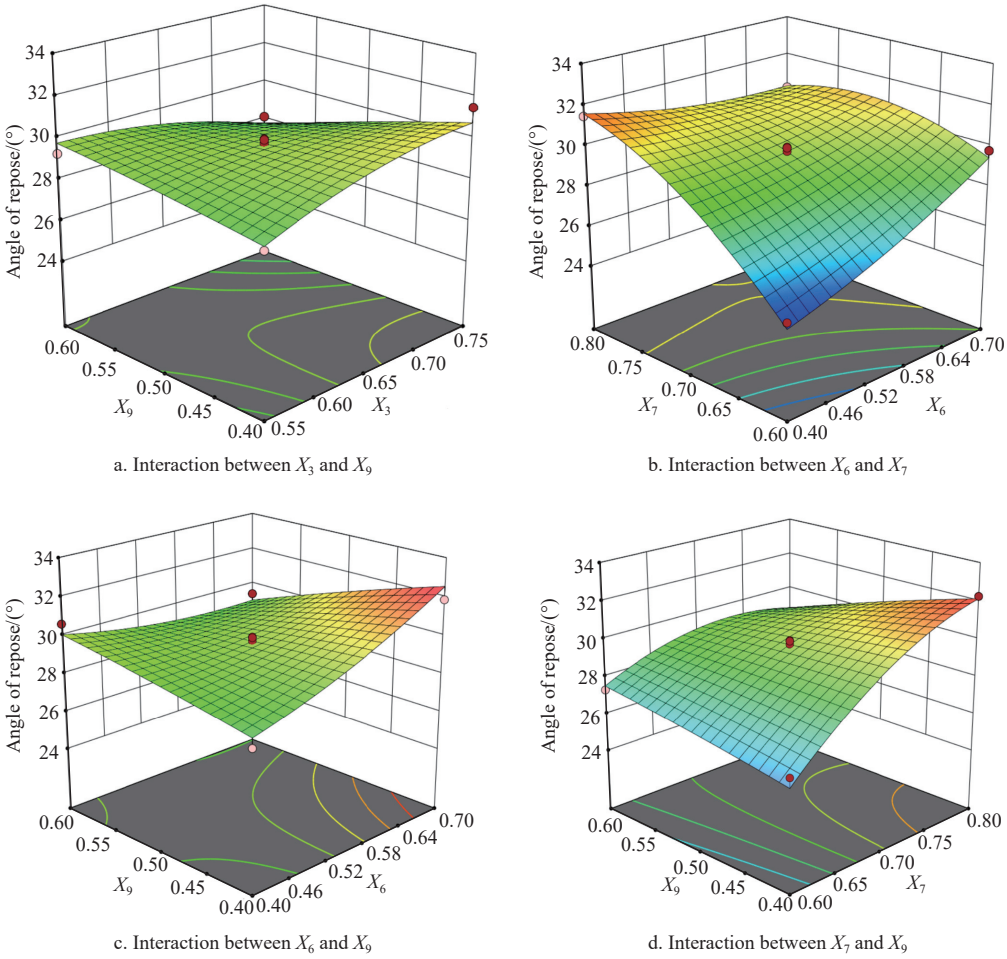

a. Interaction between X_3 and X_9

b. Interaction between X_6 and X_7

c. Interaction between X_6 and X_9

d. Interaction between X_7 and X_9

Figure 7 Effect of interaction on repose angle

4.5 Optimization of residual film-soil mixture parameters and simulation validation

To determine the optimal parameter values, the optimization function within Design-Expert software was employed. The regression model was solved with the experimentally measured angle of repose (29.80°) set as the target value. This process yielded several candidate parameter combinations. Each of these combinations was then used in a verification simulation. The final, validated parameter set was chosen based on which simulation produced a pile morphology that most accurately replicated the physical test results. The optimal values were determined to be: residual film-soil rolling friction coefficient 0.61, soil-soil rolling friction coefficient 0.60, soil-steel static friction coefficient 0.68, and soil JKR surface energy 0.46 J/m^2.

4.5.1 Angle of repose verification test

A validation simulation was conducted in EDEM to confirm the accuracy of the optimized parameter set. The previously determined optimal values were input into the model, with non-significant parameters maintained at their intermediate levels[32]. Three replicate simulations were run to ensure repeatability. The resulting angles of repose were 31.56°, 30.64°, and 31.48°, yielding a mean value of 31.23°, as illustrated in Figure 8. When compared to the actual angle of repose, this average value represents a relative error of 4.58%. This result provides strong evidence for the reliability of the calibrated contact parameters.

4.5.2 Uniaxial compression molding validation test

To further validate the calibrated parameters, a simulated uniaxial compression test was conducted and compared against

experimental results (Figure 9)[33]. The simulation meticulously replicated the physical test conditions, including particle mass and indenter velocity. The resulting force-displacement data was exported from the post-processor and analyzed in Origin. The comparison revealed a strong correlation between the simulated and experimental curves, confirmed by a high coefficient of determination (R^2=0.965 46). Furthermore, the simulated peak compressive force of 850.20 N was in close agreement with the experimental value of 872.13 N, representing a relative error of only 2.58%. Collectively, these results confirm that the calibrated contact parameters for the residual film-soil mixture are accurate and suitable for constructing a discrete element simulation model.

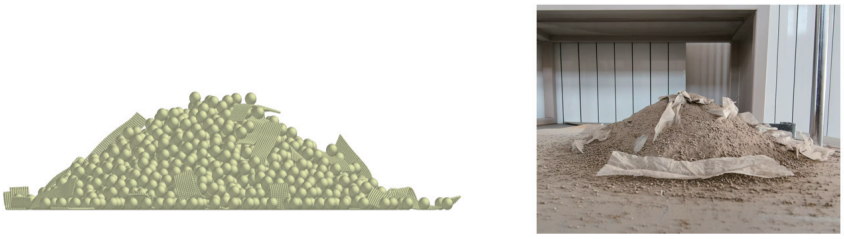

a. Simulation test b. Physical test

Figure 8 Comparison of physical test and simulation test of stacking angle

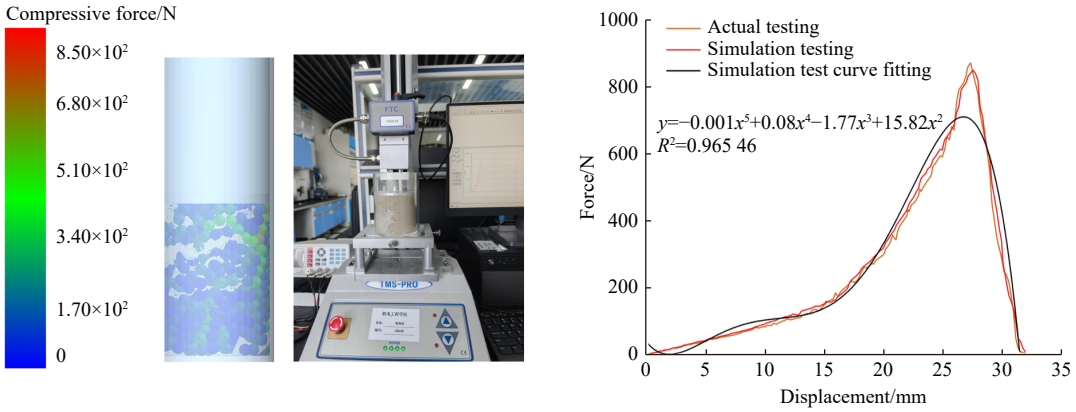

a. Verification test b. Compression force curve fitting

Figure 9 Uniaxial compression simulation test and physical test

5 Conclusions

1) A discrete element model of residual film-soil mixtures from Xinjiang cotton fields was developed in EDEM. The Hertz-Mindlin with JKR contact model was employed to simulate the mixture's behavior and calibrate its key contact parameters.

2) Integrating physical tests with simulations in Design-Expert 13.0, a Plackett-Burman experiment first identified the four most significant factors influencing the angle of repose: the soil-steel static friction coefficient (X_7), soil-soil rolling friction coefficient (X_6), residual film-soil rolling friction coefficient (X_3), and soil JKR surface energy (X_9). Subsequently, a Box-Behnken Design (BBD) was used to develop a predictive regression model linking these factors to the response. This model was then thoroughly analyzed for variance and interaction effects.

3) The optimization process yielded the final calibrated parameter set: a residual film-soil rolling friction coefficient of 0.61, a soil-soil rolling friction coefficient of 0.60, a soil-steel static friction coefficient of 0.68, and a soil JKR surface energy of 0.46 J/m^2. The reliability of this combination was confirmed through comprehensive validation testing. The relative error between the simulated and physical angle of repose was 4.58%, and the maximum relative error for the uniaxial compression test was 2.58%. These low error margins provide robust validation for the simulation model's parameters, offering a reliable foundation for future discrete element studies of soil-residual film composites. To improve the model's fidelity, future studies must incorporate the effects of moisture content on soil mechanical behavior, which is essential for constructing a scientifically-grounded discrete element model of the residual film-soil mixture.

Data availability

Data will be made available on request.

Acknowledgements

This research was supported by the Xinjiang Uygur Autonomous Region Key Research and Development Project (Grant No. 2022B02023-3), the Xinjiang Uygur Autonomous Region Competitive Bidding and Leadership Projects (Grant No. XJJBGS-MG202403), the Science and Technology Innovation Leading Talent Project of the Xinjiang Uygur Autonomous Region (Grant No. 2024TSYCLJ0014), and the Xinjiang Agricultural University Graduate Research Innovation Project (Grant No. XJAUGRI2025011).

[References]

[1] Wei X, Zhang Y P, Pan Z L, Li P C, Sun G L, Wang J, et al. The current situation and research progress of comprehensive utilization of cotton straw. Chinese Journal of Eco-Agriculture, 2025; 33(7): 1245–1260. (in Chinese)

[2] Tian X L, Cong X, Qi J T, Guo H, Li M, Fan X H. Parameter calibration of discrete element model for corn straw - soil mixture in black soil areas. Transactions of the CSAM, 2021; 52(10): 100–108, 242. (in Chinese)

[3] Zhang J X, Zhang P, Zhang H, Tan C L, Wan W Y, Wang Y C. Discrete element simulation parameters calibration for Xinjiang cotton straw.

Transactions of the CSAM, 2024; 55(1): 76–84, 108. (in Chinese)
[4] Ligier K, Vrublevskyi O, Napiorkowski J. Optimisation of calibration parameters for a discrete element method (DEM) model of plant-origin grains with a low elasticity modulus. Powder Technology, 2024; 444: 120009.
[5] Han D D, Wang Q, Tang C, Li W, Xu Y. Calibration of the contact parameters for soybean bonded particle model based on discrete element method. Journal of Mechanical Science and Technology, 2025; 39: 1279–1287.
[6] Shi R J, Dai F, Zhao W Y, Zhang F W, Shi L R, Guo J H. Establishment of discrete element flexible model and verification of contact parameters of flax stem. Transactions of the CSAM, 2022; 53(10): 146–155. (in Chinese)
[7] Du Z, Li D H, Li X P, Jin X, Wu Y B, Yu F. Calibration and experiment of discrete element model parameters for tea stem. Transactions of the CSAM, 2025; 56(1): 311–320. (in Chinese)
[8] Han D L, Hu J R, Liu H R, Ren L Z, Zhou M L, Yang Q Z, et al. Parameter calibration and experiment of the discrete element contact model of water-containing sandy soil particles. Transactions of the CSAE, 2025; 41(8): 70–78. (in Chinese)
[9] Ma S, Xu L M, Yuan Q C, Niu C, Zeng J, Chen C, et al. Calibration of discrete element simulation parameters of grapevine antifreezing soil and its interaction with soil-cleaning components. Transactions of the CSAE, 2020; 36(1): 40–49. (in Chinese)
[10] Ma Y C, Qi Y, Wang H Y, Teng D, Chen J Q, Liu D. Discrete element simulation parameter calibration and experiment of corn straw-cow manure mixture. Transactions of the CSAM, 2024; 55(12): 441–450, 504. (in Chinese)
[11] Yao W Y. Research on active anti-blocking technology of no-tillage seeding of corn in wheat-corn rotation area. PhD dissertation. Shandong University of Technology, 2023; 141p. (in Chinese)
[12] Zhang Z D, Bao G C, Yuan Y W, Lv Z Y, Chen X X, Tao C S, et al. The calibration and validation of discrete element model contact parameters for the soil-white radish root-petiole- clamping device system during the harvesting period. Computers and Electronics in Agriculture, 2025; 239: 111069.
[13] Liu Z C, Yan J G, Liu F, Wang L J. Calibration and testing of discrete element simulation parameters for the presoaked *cyperus esculentus* L. rubber interface using EDEM. Agronomy, 2025; 15(10): 2440.
[14] Wang J J, Geng B L, Yang Z K, Yang J L, Zhang K P, Meng Y R. Discrete meta-modeling and parameter calibration of harvested alfalfa stalks. Agronomy, 2025; 15(10): 2390.
[15] Zhang Z D, Bao G C, Yuan Y W, Lv Z Y, Chen X X, Chen X D, et al. Mechanical properties of radish petioles and calibration of cohesion parameters in discrete element models. Frontiers in Plant Science, 2025; 16: 1634962. doi: 10.3389/fpls.2025.1634962.
[16] Ma X T, You Y, Yang D Q, Wang D C, Hui Y T. Discrete element parameter calibration of compound fertilizer used in Camellia oleifera planting areas. Journal of Mechanical Science and Technology, 2025; 39: 5997–6009.
[17] Yue Y, Xing R S, Yasenjiang B, Xu H D, Ma W B, Guo L H. Systematic calibration and validation of discrete element model parameters for cotton root systems. Agriculture, 2025; 15(17): 1827.
[18] Peng Q J, He X, Li G M, Yang R S, Wang X Y, Zhang C Y, et al. Calibrating and testing the discrete element parameters for peanut seedling film. Int J Agric & Biol Eng, 2024; 17(5): 65–72.
[19] Zhang Z G, Zeng C, Xing Z Y, Xu P, Guo Q F, Shi R M, et al. Discrete element modeling and parameter calibrationof safflower biomechanical properties. Int J Agric & Biol Eng, 2024; 17(2): 37–46.
[20] Zhang X J, Wang H T, Wang F Y, Lian Z G. Parameter calibration of discrete element model for alfalfa seeds based on EDEM simulation experiments. Int J Agric & Biol Eng, 2024; 17(3): 33–38.
[21] Su Y, Xu Y, Cui T, Gao X J, Xia G Y, Li Y B, et al. Determination and interpretation of bonded particle model parameters for simulation of maize kernels. Biosystems Engineering, 2021; 210: 193–205
[22] Ding X T, Wang B B, He Z, Shi Y G, Li K, Cui Y J, et al. Fast and precise DEM parameter calibration for Cucurbita ficifolia seeds. Biosystems Engineering, 2023; 236: 258–276.
[23] Wang Y X, Wang X Y, Li H W, Wu Z Y, Gao S J, Liu D. Calibration of parameters for sodic saline - alkali soil discrete element model based on yield resistance. Transactions of the CSAM, 2025; 56(1): 301–310, 365. (in Chinese)
[24] Li Y J, Chen Y Y, Sun X, Lin H, He J. Parameter calibration of the breakable flexible fiber model for maize stovers with different moisture contents. Transactions of the CSAE, 2025; 41(3): 43–52. (in Chinese)
[25] Wang D W, Lu T, Zhao Z, Shang S Q, Zheng S, Liu J. Calibration of discrete element simulation parameters for cultivated soil layer in coastal saline alkali soil. Transactions of the CSAM, 2024; 55(11): 240–249. (in Chinese)
[26] Shan H Y, Yan Y N, Shen Y, Liu X J, Zhang J, Han X, et al. Calibration of discrete element parameters in wheat-corn farming straw mixed soil returning mode. Agricultural Engineering, 2024; 14(8): 72–81. (in Chinese)
[27] Qiao Y, Huang S H, Yang C Y, Liu S L, Wang K L, Lu Y P, et al. Calibration and testing of discrete element simulation parameters for ultrasonic vibration-cutter-soil interaction model. Agriculture, 2024; 15(1): 20.
[28] Chen Z F, Duan A X, Liu Y, Zhao H Q, Dai C Y, Hu S, et al. Discrete element contact model and parameter calibration of sticky particles and agglomerates. Journal of Terramechanics, 2024; 116: 100998.
[29] Chen Z F, Che G, Wan L, Wang H C, Zhang K. Calibration and experimental validation of discrete element parameters for long-grain rice with different moisture contents based on repose angle. Agriculture, 2025; 15(10): 1058.
[30] Zhang F K, Yangdao R, Wang Y L, He R H, Li P. Calibration of contact parameters of fresh-eating jujube based on discrete element method: Yuancui jujube in brittle ripe stage. International Journal of Food Properties, 2024; 27(1): 1–18.
[31] Wang X Z, Zhai Q H, Zhang S H, Li Q W, Zhou H M. Efficient and accurate calibration of discrete element method parameters for black beans. Agronomy, 2024; 14(12): 2803.
[32] Zhou H, Li D, Liu Z Y, Li Z Y, Luo S C, Xia J F. Simulation and experiment of spatial distribution effect after straw incorporation into soil by rotary burial. Transactions of the CSAM, 2019; 50(9): 69–77. (in Chinese)
[33] Li H, Meng Y B, Qi X D, Wang Y J, Li Y Q, Li M Y. Discrete element modelling method and parameter calibration of garlic species based on bonding V2 model. Transactions of the CSAM, 2025; 56(7): 150–157, 169. (in Chinese)